Discover Oncology

Research

VSV-CHIKV activates antitumor immunity by inducing pyroptosis in a melanoma model

Fan Wu[1,2] · Ying Zhan[1,2] · Siyu Wang[3] · Xiaoke Wang[1,5] · Min Hui[2,4] · Jian Zhang[5] · Jing Zhang[2] · Hongxu Yang[2] · Yingfeng Lei[5] · Shibin Yu[2]

Received: 12 February 2025 / Accepted: 22 May 2025
Published online: 29 May 2025

Abstract

Melanoma is the most dangerous skin cancer due to its difficulty in treatment, high recurrence rate and metastatic ability. As a vector for oncolytic viruses (OVs), vesicular stomatitis virus (VSV) has been shown to be effective against malignant melanoma. However, the glycoprotein G protein of VSV has potential neurotoxicity. It has been shown that replacing glycoprotein G with E3-E2-6K-E1 of chikungunya virus (CHIKV) reduces its neurotoxicity and targets gliomas. Therefore, the aim of this study was to investigate the oncolytic effect of recombinant VSV-CHIKV on melanoma and the underlying mechanism. In this study, we found that recombinant VSV-CHIKV triggered GSDMD-mediated melanoma cell pyroptosis. Importantly, the NLRP3/Caspase-1/GSDMD axis was activated after VSV-CHIKV infection in melanoma cell lines and in a xenograft mouse model. Inhibition of GSDMD blocked cell pyroptosis, antitumor immunity and the tumor response in response to VSV-CHIKV treatment, suggesting that VSV-CHIKV act through the GSDMD pathway. VSV-CHIKV-triggered GSDMD-mediated tumor pyroptosis recruited cytotoxic T lymphocytes (CTLs) into the tumor microenvironment, which was accompanied by the release of inflammatory mediators. This remodeled the tumor microenvironment and turned immunologically "cold" tumors into "hot" tumors, thereby sensitized these tumors to checkpoint blockade. Finally, the combination therapy of VSV-CHIKV and an immune checkpoint inhibitor (anti-PD-1) prolonged the survival of mice. In conclusion, the VSV-CHIKV strategy is an attractive biologic therapy against melanoma.

Keywords Oncolytic virus · Vesicular stomatitis virus · Melanoma · Pyroptosis

Fan Wu, Ying Zhan and Siyu Wang these authors contributed equally.

Supplementary Information The online version contains supplementary material available at https://doi.org/10.1007/s12672-025-02788-6.

✉ Yingfeng Lei, yflei@fmmu.edu.cn; ✉ Shibin Yu, yushibin@fmmu.edu.cn | [1]College of Life Sciences, Northwest University, Xi'an, Shannxi, China. [2]State Key Laboratory of Oral & Maxillofacial Reconstruction and Regeneration, National Clinical Research Center for Oral Diseases, Shaanxi International Joint Research Center for Oral Diseases, Department of Oral Anatomy and Physiology, School of Stomatology, The Fourth Military Medical University, Xi'an, Shaanxi, China. [3]School of Stomatology, Guizhou Medical University, Guiyang 561113, Guizhou, China. [4]College of Medicine, Northwest University, Xi'an, Shannxi, China. [5]Department of Microbiology, School of Preclinical Medicine, The Fourth Military Medical University, Xi'an, Shaanxi, China.

1 Introduction

Melanoma is a malignant tumor caused by melanocytes, which are melanin-producing cells found mainly in the skin but also in the eye, ear, hook telangiectasia, gastrointestinal tract, and mucous membranes of the oral cavity, genitals and sinuses [1]. As the most aggressive skin tumor, melanoma has a high degree of malignancy, extensive early metastasis, and extreme difficulty in clinical treatment [2]. Although melanoma accounts for only 4% of all skin cancers, it is responsible for 80% of skin cancer deaths. To date, the incidence of melanoma has been increasing globally [3].

OVs are tumor-killing viruses that can specifically infect tumor cells and replicate in large numbers in tumor cells, eventually lysing tumor cells. Because of its ability to infect and kill tumor cells, OVs has become a new direction of tumor therapy research [4, 5]. T-Vec is a genetically modified type-1 herpes simplex virus (HSV-1) that proliferates in tumor cells and expresses the immune-activating protein granulocyte macrophage colony stimulating factor (GM-CSF) [6]. T-Vec is capable of lysing melanoma cells, leading to the release of melanoma-derived antigens and GM-CSF, which accelerate the generation of a tumor-specific immune response [7]. In 2015, the Food and Drug Administration (FDA) first approved T-Vec for the treatment of locally unresectable lesions in patients with recurrent malignant melanoma. T-Vec is also the first oncolytic virus therapy drug approved by the FDA [8]. However, in a phase III clinical trial evaluating T-VEC for the treatment of melanoma patients, the objective response rate was only 26.4%, so there is an urgent need to investigate novel oncolytic viruses to improve treatment outcomes [9].

Currently, the main oncolytic viral vectors tested in clinical trials are vesicular stomatitis virus (VSV), adenovirus, herpes simplex virus, and cowpox virus [8]. VSV has many advantages as an oncolytic virus vector, including the ability to produce high-titer progeny viruses in a short time, the ability to manipulate genetic engineering easily and the ability to carry out targeted modification [10]. VSV is an enveloped negative single-stranded RNA virus of the *Rhabdoviridae* family. VSV contains five structural proteins, namely, nucleoprotein (N), phosphorylated protein (P), RNA polymerase (L), matrix protein (M), and glycoprotein (G). One of these proteins, glycoprotein G of vesicular stomatitis virus (VSV), is highly neurotropic and can lead to deleterious neurotropic consequences, including death [11]. Therefore, further modification and optimization of wild-type VSV are needed. CHIKV has a single, positive-sense, 11.8-kb RNA genome, which encodes five structural proteins (C, E3, E2, 6K, and E1). E2 underlies receptor binding, and E1 is responsible for the low pH membrane fusion activity after endocytotic entry [12, 13]. Together E2 and E1 constitute spike-like trimers on the virus surface. E3 is postulated to prevent premature virus fusion [14], and 6K enhances virion release and titer [15]. A previous study reported that by embedding the polyprotein E3-E2-6K-E1 gene of chikungunya virus into the VSV genome and replacing the VSV glycoprotein gene, the modified virus was found to have the ability to target and destroy gliomas [16]. Therefore, these modified VSV-CHIKV strains may lead to new hope for tumor therapy.

Most oncolytic viruses can induce pyroptosis, which activates an immune response that stimulates antitumor immunity [17]. Pyroptosis is a newly discovered mode of programmed cell death in inflammatory cells that is driven by inflammasome-mediated activation of various caspases, including Caspase-1, resulting in the shearing and multimerization of various gasdermin family members, including GSDMD, leading to cell perforation and cell death. Pyroptosis occurs more rapidly than apoptosis and is accompanied by the release of large amounts of proinflammatory factors [18–20]. Therefore, the development of OVs that effectively and specifically target tumor cell pyroptosis while maintaining low toxicity to normal tissues is urgently needed.

This study investigated whether VSV-CHIKV is effective against melanoma cells and the potential role and mechanism by which VSV-CHIKV induces pyroptosis.

2 Materials and methods

2.1 Cell culture

The BHK-21 cell line (CL-0034, Procell, China) was cultured in Dulbecco's modified Eagle's medium (CORNING, USA) supplemented with 10% (v/v) fetal bovine serum (Cell-Box, China) and 1% (v/v) penicillin—streptomycin (Cytiva, USA) in a water-saturated atmosphere of 5% CO_2 at 37 °C. In literature, the B16 is the most widely used and representative melanoma cell line in mice [21, 22], so it was chosen in the present study. The B16 cell line (CL-0029, Procell, China)

was cultured in high-glucose DMEM (Procell, China) containing 10% (v/v) fetal bovine serum and 1% (v/v) penicillin—streptomycin in a water-saturated atmosphere of 5% CO_2 at 37 °C.

2.2 VSV-CHIKV construction, propagation, purification and observation

The chimeric rVSV-CHIKV-EGFP was prepared according to our previous report doi: (https://doi.org/10.1038/s41541-024-00814-2). The plasmid-bearing VSV antigenome lacking VSV-G but with an additional GFP gene was synthesized at GenScript (Nanjing, China), named by VSV-ΔG. The codon-optimized E3-E2-6K-E1 gene of CHIKV (FJ959103.1) was amplified using PCR and cloned into the VSV-ΔG through homologous recombination, resulting in the rVSV-CHIKV-E3-E2-6K-E1-GFP vector. BHK-21 cells were inoculated with a vaccinia virus bearing T7 RNA polymerase (VV-T7), kindly provided by the Wuhan Institute of Virology, CAS, followed by co-transfection of five plasmids: rVSV-CHIKV- E3-E2-6K-E1-GFP vector, together with VSV accessory plasmids encoding VSV-N, VSV-P, VSV-L, and VSV-G gene, all of which were under T7 promoter control. The culture supernatant containing rVSV-CHIKV- E3-E2-6K-E1-GFP was collected 72 h post transfection and used to infect BHK cells. To reduce the neurotoxicity of VSV, the glycoprotein G gene was replaced with the E3-E2-6K-E1 gene of CHIKV (Fig. 1A). VSV-CHIKV was propagated in BHK cells. Briefly, at 80% confluence, BHK cells were inoculated with VSV-CHIKV recombinants for 2 h at 37 °C in FBS-free medium, after which complete culture medium was added for further culture. Supernatants of cell's monolayers showing cytopathic effects (CPEs) were collected. The

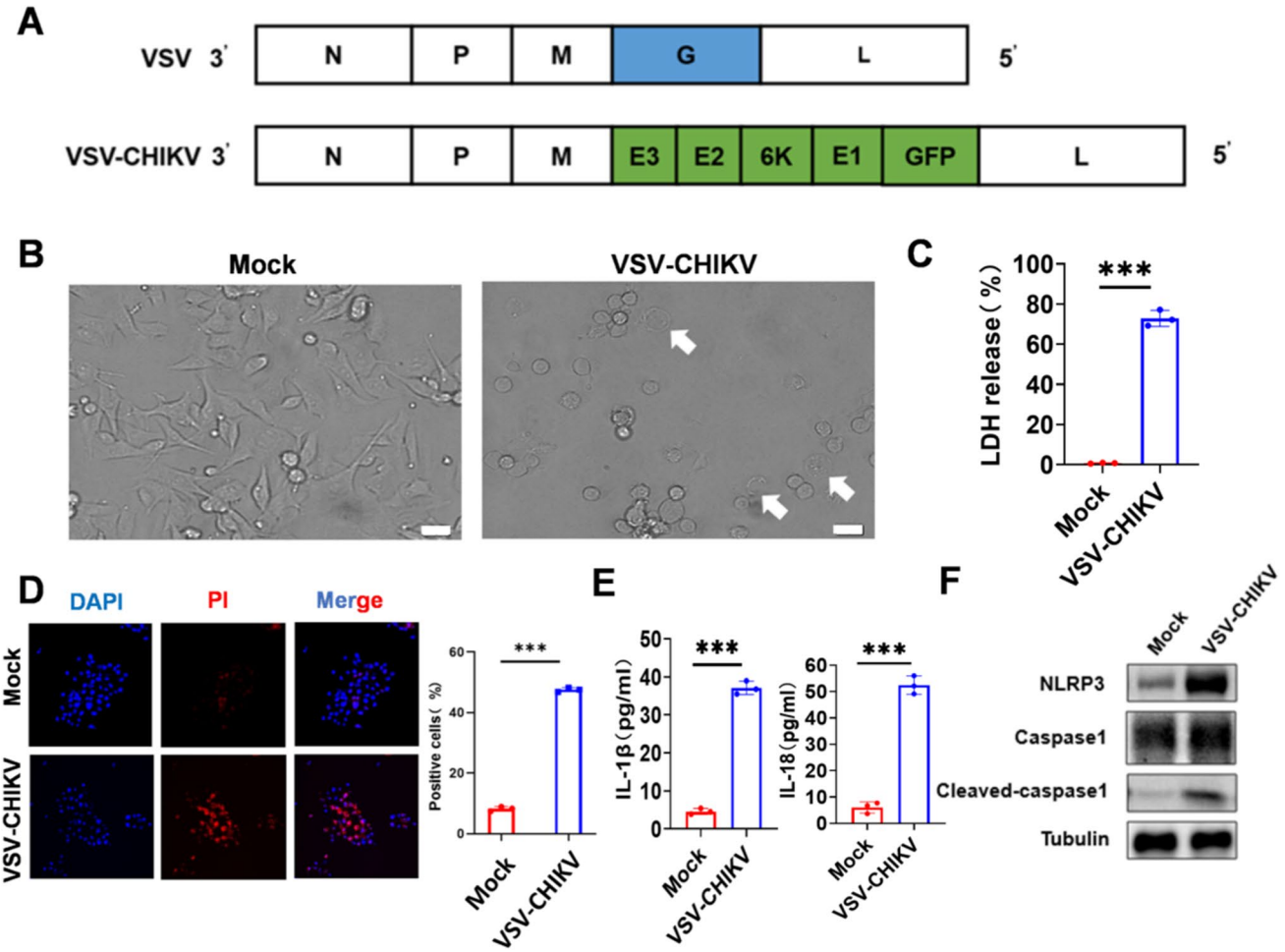

Fig. 1 Oncolytic VSV-CHIKV induces melanoma cell death (MOI = 1, 24 h). **A** Schematic showing the wild-type VSV and chimeric VSV-CHIKV genomes, in which the VSV glycoprotein G gene (blue) is replaced by the chikungunya glycoprotein sequence in the CHIKV structural polyprotein (green). **B** Images obtained by microscopy showing changes in VSV-CHIKV infection of B16 cells (scale bar: 20 μm). **C** LDH release from the culture supernatant of B16 cells infected with VSV-CHIKV (n = 3). ***$P < 0.001$ by t test. **D** Fluorescence microscopy observation of PI uptake in B16 cells (scale bars: 50 μm). ***$P < 0.001$ by t test. **E** The levels of IL-1β and IL-18 in the cell culture supernatant (n = 3). ***$P < 0.001$ by t test. **F** Western blot analysis of NLRP3, Caspase1, and Cleaved-caspase1 protein expression after the addition of VSV-CHIKV

released viruses were then purified at 4 °C and at 130,000×*g* for 2 h. The virus pellet was dissolved in Tris–EDTA (TE) buffer overnight at 4 °C and stored separately at − 80 °C.

2.3 Cell pyroptosis analysis

A total of 2×10^5 B16 cells were seeded into 6-well plates with high-glucose DMEM containing 10% (v/v) FBS at 37 °C for 24 h. Next, the culture medium in each well was washed with PBS, and fresh medium was added. The experiment involved four different groups: mock, VSV-CHIKV (MOI = 1), VSV-CHIKV (MOI = 1) + Vehicle and VSV-CHIKV (MOI = 1) + the GSDMD inhibitor LDC7559 (10 μM). LDC7559 (MedChemExpress, USA) was diluted in 10% DMSO and 90% corn oil before use. Among them, VSV-CHIKV, VSV-CHIKV + Vehicle and VSV-CHIKV + LDC7559 were filtered through a 0.22 μm sterile filter membrane and added to B16 cells for 24 h. Images of pyroptotic cells with air bubbles were observed via optical microscopy. LDH release was used to detect the integrity of the cell membranes and was assessed according to the manufacturer's instructions (Beyotime, China). Culture supernatants were collected, and the levels of the inflammatory factors IL-1β and IL-18 were detected via ELISA according to the manufacturer's instructions (Servicebio, China).

2.4 Animal tests

C57BL/6 male mice (6 weeks of age and weighing 20–22 g) were provided by the Animal Center of Fourth Military Medical University. All procedures adhering to the ARRIVE guidelines were examined and approved by the Institutional Ethics Committee of the School of Stomatology, Fourth Military Medical University (kq-2022-020). All surgeries were performed under sodium pentobarbital anesthesia, and all efforts were made to minimize suffering. A total of 3×10^6 B16 cells were implanted subcutaneously into the right dorsal side of C57BL/6 mice. When the tumors were visible, the length (L) and width (W) of each tumor were measured daily with calipers, and the tumor volume was calculated using the following formula: $(L \times W^2)/2$. Twelve days after the injection of tumor cells, VSV-CHIKV (1 × 10^6 PFU in a volume of 10 μL) or VSV-CHIKV (1 × 10^6 PFU in a volume of 10 μL) + LDC7559 (10 mg/kg) was injected within the tumor every two days for a total of five injections (Fig. 3A, 4A). Tumor tissues were taken from each mouse for ELISA, immunohistochemistry, Western blotting, PCR and flow cytometry. The heart, liver, spleen, lungs and kidneys were removed for hematoxylin and eosin (H&E) staining. For HE and immunohistochemical analyses, tissue blocks were extracted, fixed in 4% paraformaldehyde for 24 h and embedded in paraffin. Then, the tissue samples were embedded in paraffin blocks and sectioned at 5 μm thickness.

To investigate the efficacy of the treatment of VSV-CHIKV in combination with PD-1 blockade, 12 days after the injection of tumor cells, PBS or VSV-CHIKV (1 × 10^6 PFU in a volume of 10 μL) was injected into the tumor first, and IgG or aPD-1 (5 mg/kg) was injected intraperitoneally every other day for a total of 5 injections (Fig. 6A). In VivoMab-conjugated anti-mouse PD-1 (CD279) (BE0146) was purchased from BioXCell.

2.5 Histology and immunohistochemical staining

The serial sections were stained with HE as reported previously [23]. IHC staining was performed by avidin–biotin complex (ABC) staining. In brief, after deparaffinization, hydration and blockage of endogenous peroxidase, the sections were incubated with 5% goat serum to block specific sites and then incubated overnight with the following primary antibodies: anti-NLRP3 antibody (68102-1-Ig, Proteintech, USA), anti-Caspase1 antibody (sc-56036, Santa Cruz Biotechnology, USA), anti-cleaved caspase 1 antibody (AF4022, Affinity, USA), anti-GSDMD antibody (ab219800, Abcam, UK) and anti-GSDMD-N antibody (DF13758, Affinity, USA). After rinsing, the sections were incubated with biotinylated conjugated goat anti-rabbit or donkey anti-goat secondary antibody and then incubated with 3,3′-diaminobenzidine tetrahydrochloride (DAB) substrate for 30 s to 2 min for different antibodies. Sections were mounted with balsam after being dehydrated in serial alcohol solutions. Images were acquired using a Leica DFC490 system under a light microscope (DM 2500, Wetzlar, Germany).

2.6 Immunofluorescence

B16 cells were stained with immunofluorescence to evaluate the expression of GSDMD-N. Cells were incubated with primary antibody against GSDMD-N on round, sterilized glass cover slips (14 mm) and then incubated with Cy3-labeled secondary antibody diluted with DAPI for 2 h. Cover slips were placed on clean slides, sealed with antifluorescence

quenching sealing liquid, stored at 4 °C and then observed by confocal laser scanning microscopy (Olympus, FV1000, Tokyo, Japan).

2.7 Flow cytometry

Tumor tissue samples were collected, minced and separated into homogenates with type I collagenase (1 mg ml^{-1}; Worthington, China) on a shaker at 37 °C and 220 rpm for 1 h. The homogenate was filtered through a nylon mesh filter and washed with PBS. Erythrocyte lysate was added, and the samples were lysed at 4 °C for 15 min and then centrifuged and washed with PBS. To analyze the presence of active T cells in tumors, single-cell suspensions were incubated with PE-conjugated anti-CD4 (100408, Biolegend, USA), APC-conjugated anti-CD8 (100765, Biolegend, USA) or FITC-conjugated anti-CD3 (100306, Biolegend, USA) for 30 min at 4 °C. To further evaluate the expression of PD-1 and PD-L1 in the tumour tissues of the mock and VSV-CHIKV-treated groups, single-cell suspensions were incubated with APC Rat IgG2a, κ Isotype Control(E-AB-F09832E, Elabscience, China), APC Anti-Mouse CD279/PD-1 Antibody (E-AB-F1131E, Elabscience, China), APC Rat IgG2b, κ Isotype Control(E-AB-F09842E, Elabscience, China) or APC Anti-Mouse CD274/PD-L1 Antibody (E-AB-F1132E, Elabscience, China) for 30 min at 4 °C. The data were analyzed with a Beckman CytoFLEX (Beckman Coulter) instrument, and the data were analyzed using FlowJo V10 software.

2.8 RT-qPCR analysis

Total RNA was extracted from tumor tissues and cells with TRIzol (Invitrogen, China). All the genes were analyzed using CFX96 real-time PCR (Bio-Rad, USA). The sequences of primers used were designed and synthesized based on the mRNA sequences obtained from the NCBI database, in Table 1. The expression of each target gene was analyzed three times relative to that of GAPDH, and the mean values were calculated using the $2^{-\Delta\Delta Ct}$ method.

2.9 Western blotting

Isolated cells and tissues were subjected to RIPA lysis buffer (NCM Biotech, China) supplemented with ProtLytic Protease and Phosphatase Inhibitor Cocktail (NCM Biotech, China), and the protein concentration was detected with a BCA protein assay kit. Equal amounts of proteins from each group were separated by 10% sodium dodecyl sulfate—polyacrylamide gel electrophoresis and transferred to polyvinylidene fluoride (PVDF) membranes. The membranes were blocked in BSA for 1 h and then incubated overnight with primary antibodies against NLRP3, Caspase 1, Cleaved-caspase 1, GSDMD, GSDMD N-terminal and β-tubulin (AF7011, Affinity, USA) at 4 °C. The membranes were then incubated with a 1:2000 dilution of HRP-conjugated Affinipure goat anti-rabbit IgG (H + L) (SA00001-2, Proteintech, USA) or HRP-conjugated Affinipure goat anti-mouse IgG (H + L) (SA00001-1, Proteintech, USA) for 1 h at RT. A SuperSignal West Pico chemiluminescent substrate kit (Thermo Scientific, Rockford, IL) was used to visualize the blots according to the manufacturer's instructions. Then, the membranes were scanned with a ChemiDoc XRS + WB luminous imaging system. Image Lab 5.2.1 software was used for analysis after image acquisition.

2.10 Statistical analysis

All the data are expressed as the mean ± standard deviation (SD). The results presented are representative of at least three independent experiments and are expressed as the mean ± SD. Student's t test was used to compare the differences between two groups. A one-way analysis of variance model was used to compare multiple groups, and Tukey's

Table 1 Gene primers

Gene	Forward	Reverse
IFN-γ	5′-ATGAACGCTACACACTGCATC-3′	5′-CCATCCTTTTGCCAGTTCCTC-3′
IL-2	5′-TGAGCAGGATGGAGAATTACAGG-3′	5′-GTCCAAGTTCATCTTCTAGGCAC-3′
IL-12	5′-GTCCTCAGAAGCTAACCATCTCC-3′	5′-CCAGAGCCTATGACTCCATGTC-3′
TGF-β	5′-TCTGCATTGCACTTATGCTGA-3′	5′-AAAGGGCGATCTAGTGATGGA-3′
Foxp3	5′-CACCTATGCCACCCTTATCCG-3′	5′-CATGCGAGTAAACCAATGGTAGA-3′
GAPDH	5′-TGTGTCCGTCGTGGATCTGA-3′	5′-TTGCTGTTGAAGTCGCAGGAG-3′

Fig. 2 Melanoma cell pyroptosis triggered by oncolytic VSV-CHIKV is mediated by the NLRP3/Caspase-1/GSDMD axis (MOI = 1, 24 h). **A** Western blot analysis of GSDMD and GSDMD-N protein expression after the addition of VSV-CHIKV. **B** Expression of the GSDMD-N protein in the cytoplasm of cells after VSV-CHIKV infection of B16 cells. GSDMD-N, red; DAPI, blue (scale bar: 10 μm). ***$P < 0.001$ by t test. **C** Images obtained by microscopy showing changes in B16 cells after the addition of LDC7559 (scale bar: 20 μm). **D** LDH release from culture supernatants of B16 cells after the addition of LDC7559 (n = 3). ***$P < 0.001$ by One-way ANOVA. **E** Fluorescence microscopy of PI uptake in B16 cells after the addition of LDC7559 (scale bar: 50 μm). ***$P < 0.001$ by One-way ANOVA. **F** The levels of IL-1β and IL-18 in the cell culture supernatant after the addition of LDC7559 (n = 3). **$P < 0.01$, ***$P < 0.001$ by One-way ANOVA. **G** Western blot analysis of NLRP3, Caspase1, Cleaved-caspase1, GSDMD and GSDMD-N protein expression after the addition of LDC7559. **H** Expression of GSDMD-N protein in the cytoplasm of cells after the addition of LDC7559 to B16 cells. GSDMD-N, red; DAPI, blue (scale bar: 10 μm). ***$P < 0.001$ by One-way ANOVA

multiple comparisons test was used to compare 2 groups. $P < 0.05$ was considered to indicate statistical significance. All the statistical analyses were conducted with GraphPad Prism 8.0.

3 Results

3.1 Oncolytic VSV-CHIKV induces melanoma cell death

Human immunodeficiency virus (HIV) and respiratory syncytial virus (RSV) have been reported to induce immune cell pyroptosis, and influenza A virus induces epithelial cell pyroptosis [24–26]. VSV is a well-studied oncolytic virus, and it is important to explore whether recombinant VSV-CHIKV can induce tumor pyroptosis. Previous findings revealed that both green (VSV-CHIKV carries the EGFP gene) and red (VSV-CHIKV protein staining) fluorescence were expressed in VSV-CHIKV-infected B16 cells (Supplementary Fig. 1). After treating B16 cells with VSV-CHIKV (MOI = 1) for 24 h, cell membrane swelling and subsequent bubble-blowing were observed in the VSV-CHIKV group compared with the mock group (Fig. 1B). LDH release ($P < 0.001$) (Fig. 1C) and the number of PI-positive cells (Fig. 1D) were greater in the VSV-CHIKV group than in the mock group, indicating that cell membrane integrity was disrupted. In addition, the expression of IL-1β ($P < 0.001$) and IL-18 ($P < 0.001$) was greater in the VSV-CHIKV group than in the mock group, demonstrating the proinflammatory effect of VSV-CHIKV-induced cell death (Fig. 1E). Compared with those in the mock group, the protein levels of NLRP3 and as shown indemonstrated that the VSV-CHIKV strategy triggered pyroptosis in B16 cells.

3.2 Melanoma cell pyroptosis triggered by the oncolytic virus VSV-CHIKV is mediated by the NLRP3/Caspase-1/GSDMD axis

Given that caspase-1 was reported to be the determinant of GSDMD-mediated tumor cell pyroptosis [27], we wondered whether VSV-CHIKV could activate the NLRP3/Caspase-1/GSDMD axis in B16 cells. Compared with those in the mock group, the protein levels of GSDMD-N in the VSV-CHIKV group were significantly greater (Fig. 2A). Similarly, in Fig. 2B, more GSDMD-N-positive cells were found in the VSV-CHIKV group. To further elucidate the key factors involved in VSV-CHIKV-induced cellular pyroptosis, we treated colon cancer cell line (MC38) with VSV-CHIKV and similarly found activation of GSDMD-N (Supplementary Fig. 2). Compared with those in the VSV-CHIKV group and the VSV-CHIKV + Vehicle group, the cell morphology was restored, and the number of bubble-like protrusions was significantly lower in the VSV-CHIKV + LDC7559 group (Fig. 2C). Furthermore, after LDC7559 treatment, LDH release (VSV-CHIKV + LDC7559 vs VSV-CHIKV, $P < 0.001$; VSV-CHIKV + LDC7559 vs VSV-CHIKV + Vehicle, $P < 0.001$) (Fig. 2D) and the number of PI-positive cells (Fig. 2E) were reduced significantly, suggesting that cell membrane integrity was restored. In addition, compared with those in the VSV-CHIKV group and the VSV-CHIKV + Vehicle group, the levels of IL-1β (VSV-CHIKV + LDC7559 vs VSV-CHIKV, $P < 0.001$; VSV-CHIKV + LDC7559 vs VSV-CHIKV + Vehicle, $P < 0.001$) and of IL-18 (VSV-CHIKV + LDC7559 vs VSV-CHIKV, $P < 0.01$; VSV-CHIKV + LDC7559 vs VSV-CHIKV + Vehicle, $P < 0.01$) in the culture supernatant (Fig. 2F), reduced protein levels of GSDMD-N (Fig. 2G), and reduced expression in GSDMD-N-positive cells (Fig. 2H) were found in the VSV-CHIKV + LDC7559 group. The above results suggest that the oncolytic virus VSV-CHIKV induces pyroptosis in melanoma cells via the NLRP3/Caspase-1/GSDMD pathway.

3.3 Oncolytic VSV-CHIKV causes pyroptosis in a melanoma cancer model

Here, to determine whether VSV-CHIKV can function ideally in vitro and in vivo in the same way, the expression of inflammatory factors and protein levels related to pyroptosis were detected. Previous findings revealed that both green

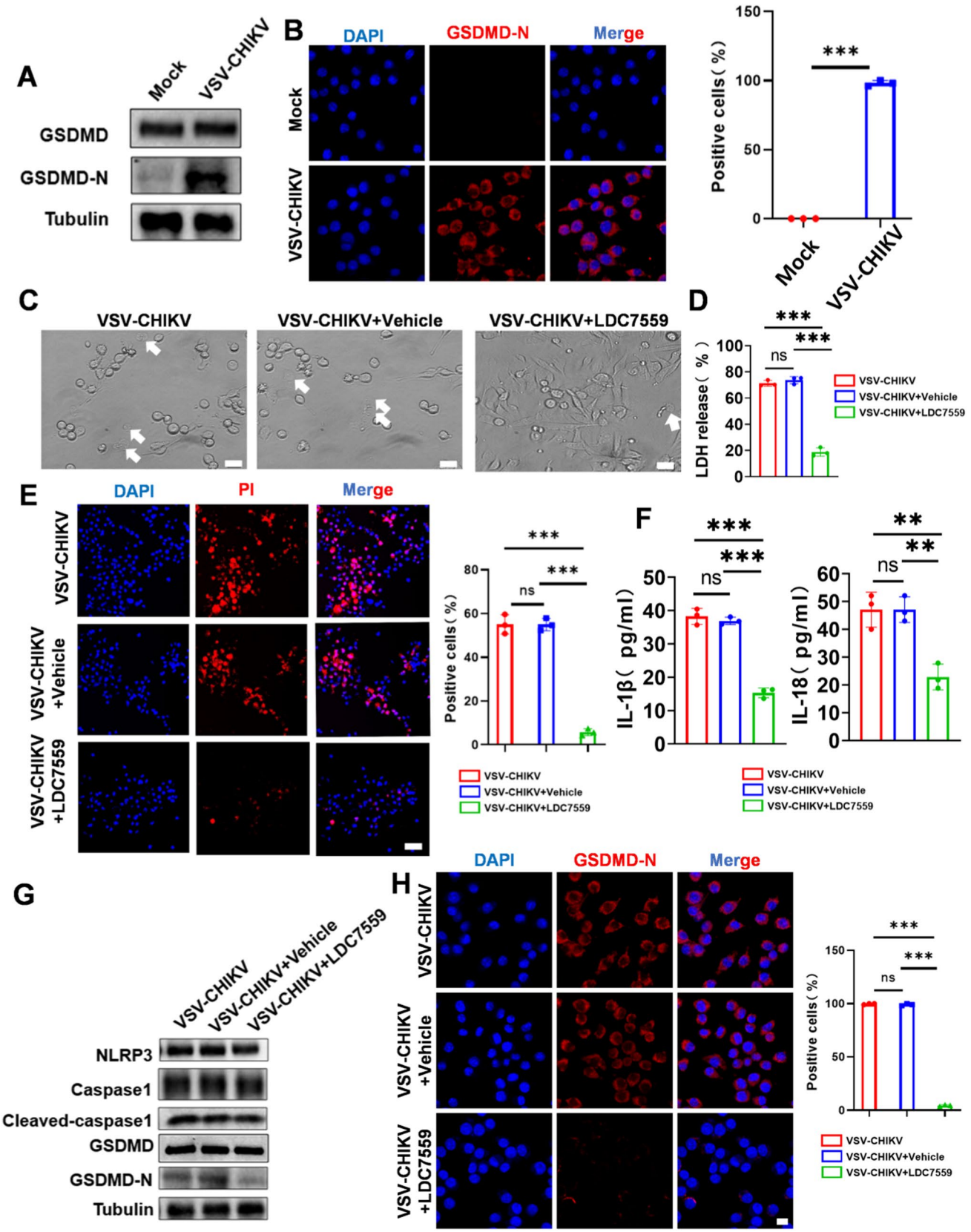
A
Mock
VSV-CHIKV
GSDMD
GSDMD-N
Tubulin
B
DAPI
GSDMD-N
Merge
Mock
VSV-CHIKV
Positive cells (%)
150
100
50
0
***
Mock
VSV-CHIKV
C
VSV-CHIKV
VSV-CHIKV+Vehicle
VSV-CHIKV+LDC7559
D
***
***
ns
LDH release (%)
100
80
60
40
20
0
VSV-CHIKV
VSV-CHIKV+Vehicle
VSV-CHIKV+LDC7559
E
DAPI
PI
Merge
VSV-CHIKV
VSV-CHIKV +Vehicle
VSV-CHIKV +LDC7559
***
***
ns
Positive cells (%)
80
60
40
20
0
VSV-CHIKV
VSV-CHIKV+Vehicle
VSV-CHIKV+LDC7559
F
***
***
ns
IL-1β (pg/ml)
50
40
30
20
10
0
**
**
ns
IL-18 (pg/ml)
60
50
40
30
20
10
0
VSV-CHIKV
VSV-CHIKV+Vehicle
VSV-CHIKV+LDC7559
G
VSV-CHIKV
VSV-CHIKV+Vehicle
VSV-CHIKV+LDC7559
NLRP3
Caspase1
Cleaved-caspase1
GSDMD
GSDMD-N
Tubulin
H
DAPI
GSDMD-N
Merge
VSV-CHIKV
VSV-CHIKV +Vehicle
VSV-CHIKV +LDC7559
***
***
ns
Positive cells (%)
150
100
50
0
VSV-CHIKV
VSV-CHIKV+Vehicle
VSV-CHIKV+LDC7559

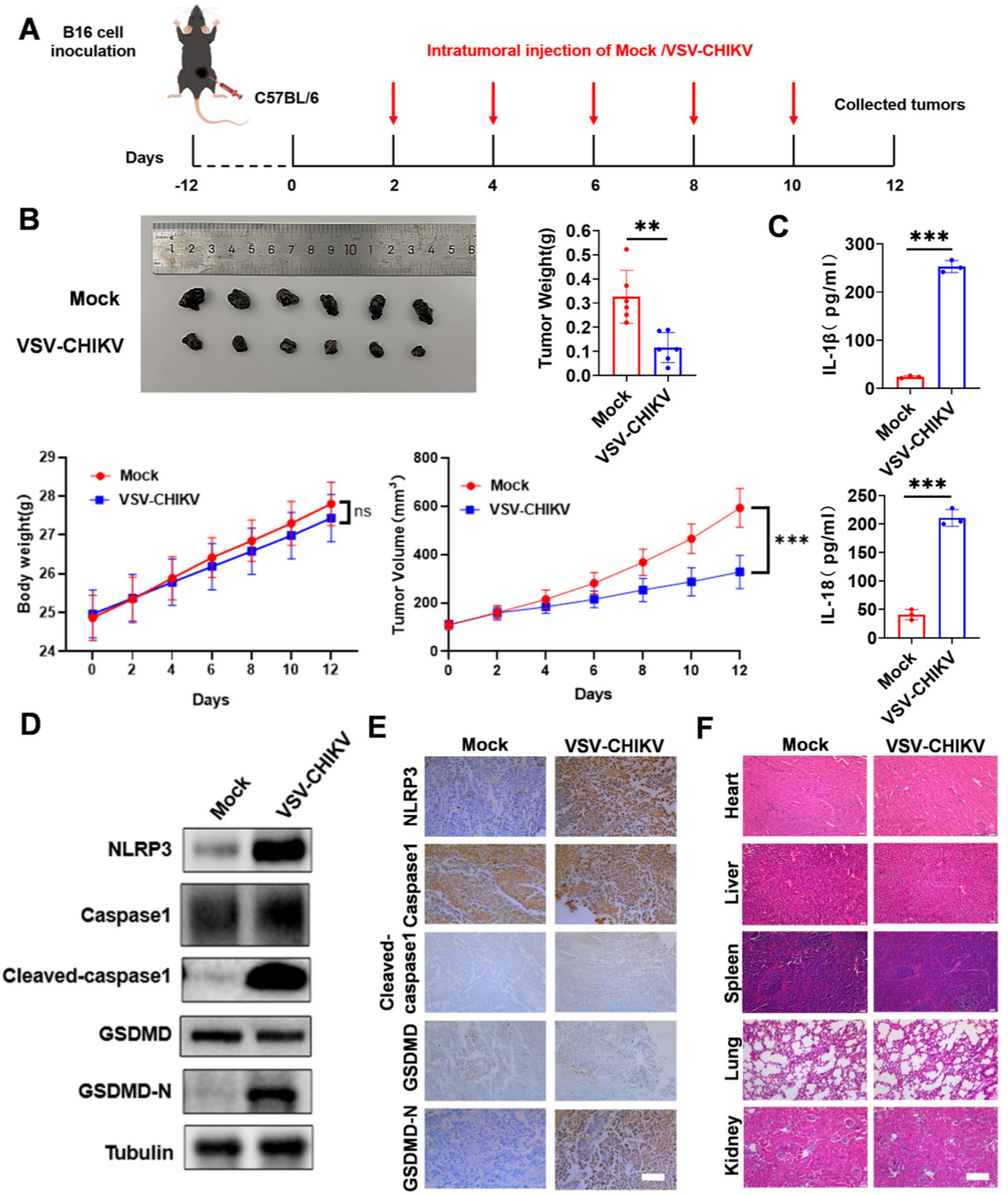

Fig. 3 Oncolytic VSV-CHIKV causes pyroptosis in a melanoma cancer model. **A** Schematic illustration of the experimental design. B16 cell tumor-bearing C57BL/6 mice were intratumorally treated with VSV-CHIKV. **B** B16 tumors collected after VSV-CHIKV infection; images of the tumors, tumors weights (n = 6), body weight (n = 6), tumors growth curves are shown. $^{**}P < 0.01$ by t test. $^{***}P < 0.001$ by t test. **C** IL-1β and IL-18 levels in tumor tissues (n = 3). $^{***}P < 0.001$ by t test. **D** NLRP3, Caspase1, Cleaved-caspase1, GSDMD and GSDMD-N proteins in the mock group and the VSV-CHIKV group determined by Western blotting. **E** Immunohistochemical staining for the NLRP3, Caspase1, Cleaved-caspase1, GSDMD and GSDMD-N proteins in the mock group and the VSV-CHIKV group (scale bar: 100 μm). **F** HE staining of major organs (scale bar: 100 μm)

(VSV-CHIKV carries the EGFP gene) and red (VSV-CHIKV protein staining) fluorescence were expressed in VSV-CHIKV-infected B16 tissues (Supplementary Fig. 3). Compared with those in the mock group, the tumor growth rate ($P < 0.01$) (Fig. 3B) and the levels of the cytokines IL-1β ($P < 0.001$) and IL-18 ($P < 0.001$) were significantly greater in the VSV-CHIKV group (Fig. 3C). However, compared with those in the mock group, the protein levels of NLRP3, cleaved caspase-1, and GSDMD-N were increased in the VSV-CHIKV group (Fig. 3D, E). There were no significant changes in major organs, such as the heart, liver, spleen, lung or kidney, after VSV-CHIKV injection (Fig. 3F). And no green fluorescence (VSV-CHIKV carries the EGFP gene) was detected in these organs, indicating that VSV-CHIKV did not infect normal organs (Supplementary Fig. 4). Taken together, these results confirm that VSV-CHIKV can be used as a strategy to induce melanoma cell pyroptosis.

3.4 Inhibition of GSDMD impairs VSV-CHIKV-induced melanoma tumor suppression

To further elucidate the relationship between VSV-CHIKV and GSDMD, we injected LDC7559 into melanoma cells. Compared with those in the VSV-CHIKV group and the VSV-CHIKV + Vehicle group, the tumor growth rate (VSV-CHIKV + LDC7559 vs. VSV-CHIKV, $P < 0.001$; VSV-CHIKV + LDC7559 vs. VSV-CHIKV + Vehicle, $P < 0.001$) (Fig. 4B) and the content of IL-1β (VSV-CHIKV + LDC7559 vs. VSV-CHIKV, $P < 0.001$; VSV-CHIKV + LDC7559 vs. VSV-CHIKV + Vehicle, $P < 0.001$) and that of IL-18 (VSV-CHIKV + LDC7559 vs. VSV-CHIKV, $P < 0.001$; VSV-CHIKV + LDC7559 vs. VSV-CHIKV + Vehicle, $P < 0.001$) were significantly lower in the VSV-CHIKV + LDC7559 group (Fig. 4C). However, compared with those in the VSV-CHIKV group and the VSV-CHIKV + Vehicle group, the protein levels of GSDMD-N were decreased in the VSV-CHIKV + LDC7559 group (Fig. 4D, E). After the injection of VSV-CHIKV, VSV-CHIKV + Vehicle or VSV-CHIKV + LDC7559, there were no significant changes in major organs, such as the heart, liver, spleen, lungs and kidneys (Fig. 4F). Taken together, these findings indicate that GSDMD is essential for vesicular stomatitis virus (VSV-CHIKV)-triggered intratumoral cytotoxic T lymphocyte recruitment and tumor suppression.

3.5 Inhibition of GSDMD impairs VSV-CHIKV-induced antitumor immunity against melanoma tumors

Given that VSV-CHIKV-induced pyroptosis has been confirmed, we further investigated the immune-stimulating ability of this viral therapy. Compared with those in the mock group, the mRNA levels of the proinflammatory factors IL-2 ($P < 0.01$), IL-12 ($P < 0.001$) and IFN-γ ($P < 0.01$) were significantly upregulated in the VSV-CHIKV group. In contrast, the expression of the anti-inflammatory factors Foxp3 ($P < 0.01$) and TGF-β ($P < 0.001$) was significantly downregulated after VSV-CHIKV infection (Fig. 5A). To further assess the immunostimulatory effects of VSV-CHIKV in vivo, the infiltration of various immune cells within melanoma tumors was detected. The proportion of $CD3^+CD8^+$ cytotoxic lymphocytes within the tumors of mice in the VSV-CHIKV group was significantly greater than that in the mock group ($P < 0.001$) (Fig. 5B). Meanwhile, we further assessed the expression of PD-1 and PD-L1 in Mock versus VSV-CHIKV-treated tumor tissues, and although both markers were highly expressed, no statistically significant differences were observed between groups (Fig. 5C). These findings provide insight into the improved efficacy of combination therapy with VSV-CHIKV and anti-PD-1 immune checkpoint blockers. Compared with those in the VSV-CHIKV group and the VSV-CHIKV + Vehicle group, the mRNA levels of the related proinflammatory factors IL-2 (VSV-CHIKV + LDC7559 vs VSV-CHIKV, $P < 0.001$; VSV-CHIKV + LDC7559 vs VSV-CHIKV + Vehicle, $P < 0.01$) and IL-12 (VSV-CHIKV + LDC7559 vs VSV-CHIKV, $P < 0.001$; VSV-CHIKV + LDC7559 vs VSV-CHIKV + Vehicle, $P < 0.001$). 001), and IFN-γ (VSV-CHIKV + LDC7559 vs VSV-CHIKV, $P < 0.01$; VSV-CHIKV + LDC7559 vs VSV-CHIKV + Vehicle, $P < 0.01$) was significantly downregulated in the VSV-CHIKV + LDC7559 group. In contrast, the expression of the anti-inflammatory factors TGF-β (VSV-CHIKV + LDC7559 vs VSV-CHIKV, $P < 0.001$; VSV-CHIKV + LDC7559 vs VSV-CHIKV + Vehicle, $P < 0.001$) and Foxp3 (VSV-CHIKV + LDC7559 vs VSV-CHIKV, $P < 0.001$; VSV-CHIKV + LDC7559 vs VSV-CHIKV + Vehicle, $P < 0.001$) was significantly upregulated in the VSV-CHIKV + LDC7559 group (Fig. 5D). Compared with those in the VSV-CHIKV group and the VSV-CHIKV + Vehicle group, the proportion of $CD3^+CD8^+$ cytotoxic lymphocytes in the tumors of the VSV-CHIKV + LDC7559 group was significantly lower (VSV-CHIKV + LDC7559 vs VSV-CHIKV, $P < 0.001$; VSV-CHIKV + LDC7559 vs VSV-CHIKV + Vehicle, $P < 0.001$) (Fig. 5E). Taken together, these results confirm that VSV-CHIKV provides the basis for tumor immunotherapy by inducing an immunogenic tumor microenvironment and promoting the expansion of tumor cytotoxic T cells.

3.6 VSV-CHIKV-based virotherapy enhances the efficacy of immune checkpoint blockade

Unlike immunologically "hot" tumors infiltrated with sufficient T cells, B16-derived tumors, which are considered immunologically "cold" tumors, generally show a poor response to PD-1 blockade therapy [28]. Indeed, we observed that

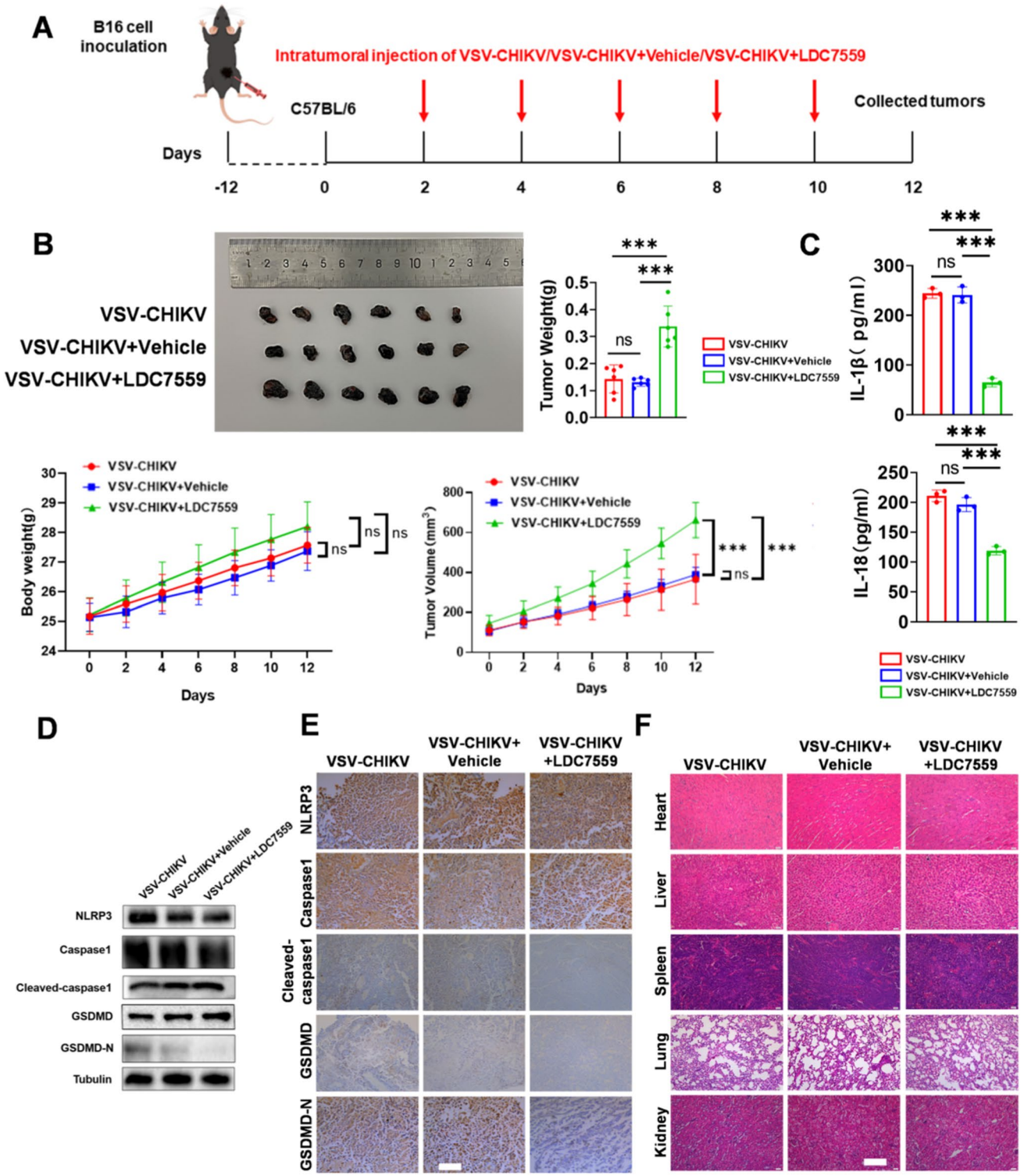

Fig. 4 Inhibition of GSDMD impairs VSV-CHIKV-induced melanoma tumor suppression. **A** Schematic illustration of the experimental design. B16 cell tumor-bearing C57BL/6 mice were intratumorally treated with VSV-CHIKV, VSV-CHIKV + Vehicle, or VSV-CHIKV + LDC7559. **B** B16 tumors from the VSV-CHIKV, VSV-CHIKV + Vehicle, and VSV-CHIKV + LDC7559 groups were collected after treatment; images of the tumors, tumors weights (n = 6), body weight (n = 6) and tumors growth curves are shown. ***$P < 0.001$ by One-way ANOVA. **C** The levels of IL-1β and IL-18 in tumor tissues (n = 3). ***$P < 0.001$ by One-way ANOVA. **D** Expression of the NLRP3, Caspase1, Cleaved-caspase1, GSDMD and GSDMD-N proteins in the VSV-CHIKV, VSV-CHIKV + Vehicle and VSV-CHIKV + LDC7559 groups determined by Western blotting. **E** Immunohistochemical staining for the NLRP3, Caspase1, Cleaved-caspase1, GSDMD and GSDMD-N proteins in the VSV-CHIKV, VSV-CHIKV + Vehicle and VSV-CHIKV + LDC7559 groups (scale bar: 100 μm). **F** HE staining of major organs (scale bar: 100 μm)

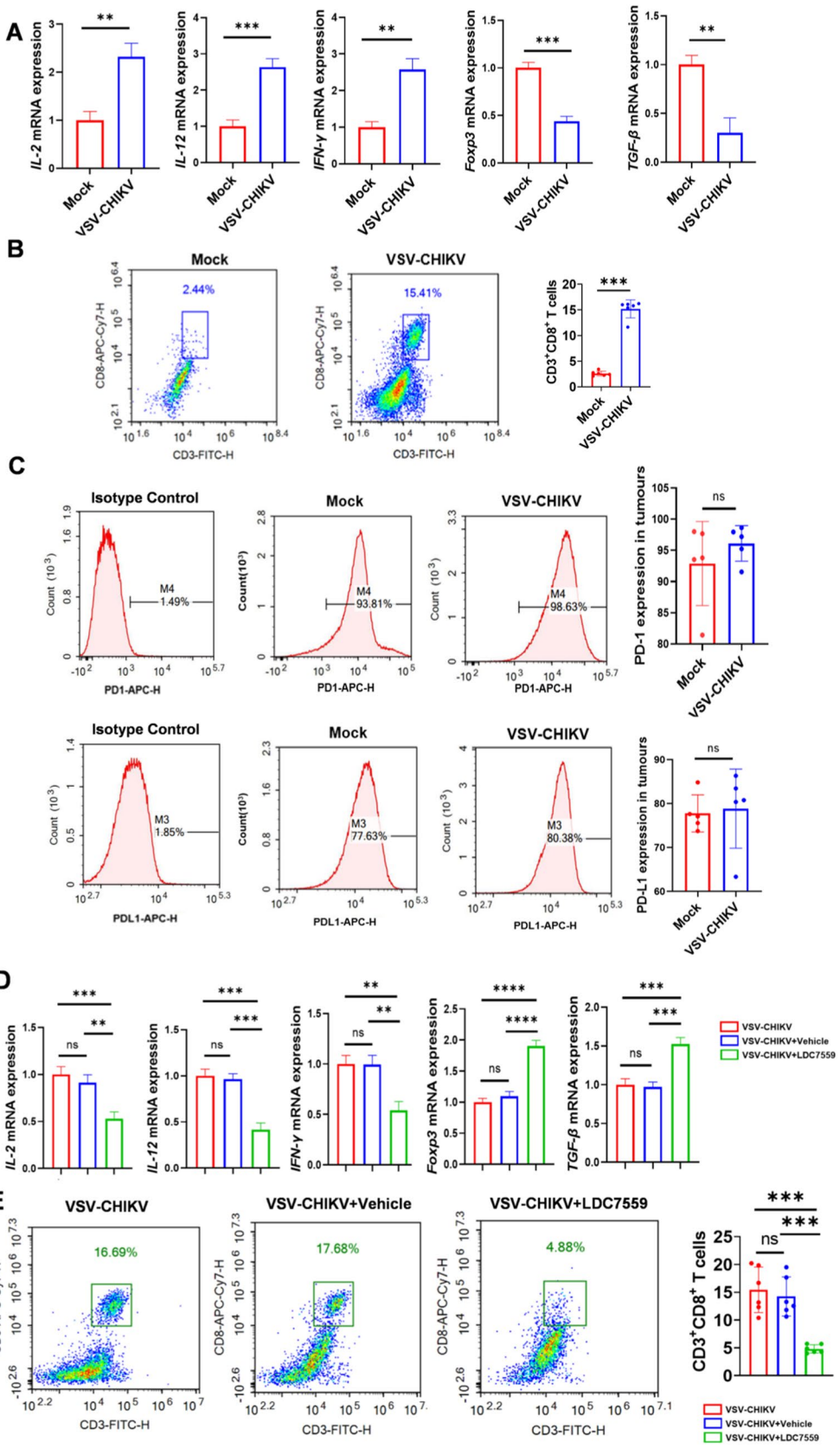

Fig. 5 Inhibition of GSDMD impairs VSV-CHIKV-induced antitumor immunity against melanoma tumors. **A** mRNA expression analysis of IL-2, IL-12, IFN-γ, TGF-β and Foxp3 in mouse tumors (n = 3). $^{**}P < 0.01$, $^{***}P < 0.001$ by t test. **B** Flow cytometry detection of $CD3^{+}CD8^{+}$ T cells expression in melanoma tissues. The results of the quantitative analysis are shown on the right (n = 6). $^{***}P < 0.001$ by t test. **C** Flow cytometry detection of PD-1 and PD-L1 expression in melanoma tissues. The results of the quantitative analysis are shown on the right (n = 5). **D** mRNA expression analysis of IL-2, IL-12, IFN-γ, TGF-β and Foxp3 in mouse tumors (n = 3). $^{**}P < 0.01$, $^{***}P < 0.001$ by One-way ANOVA. **E** Detection of $CD3^{+}CD8^{+}$ T cells by flow cytometry. The results of the quantitative analysis are shown on the right (n = 6). $^{***}P < 0.001$ by One-way ANOVA

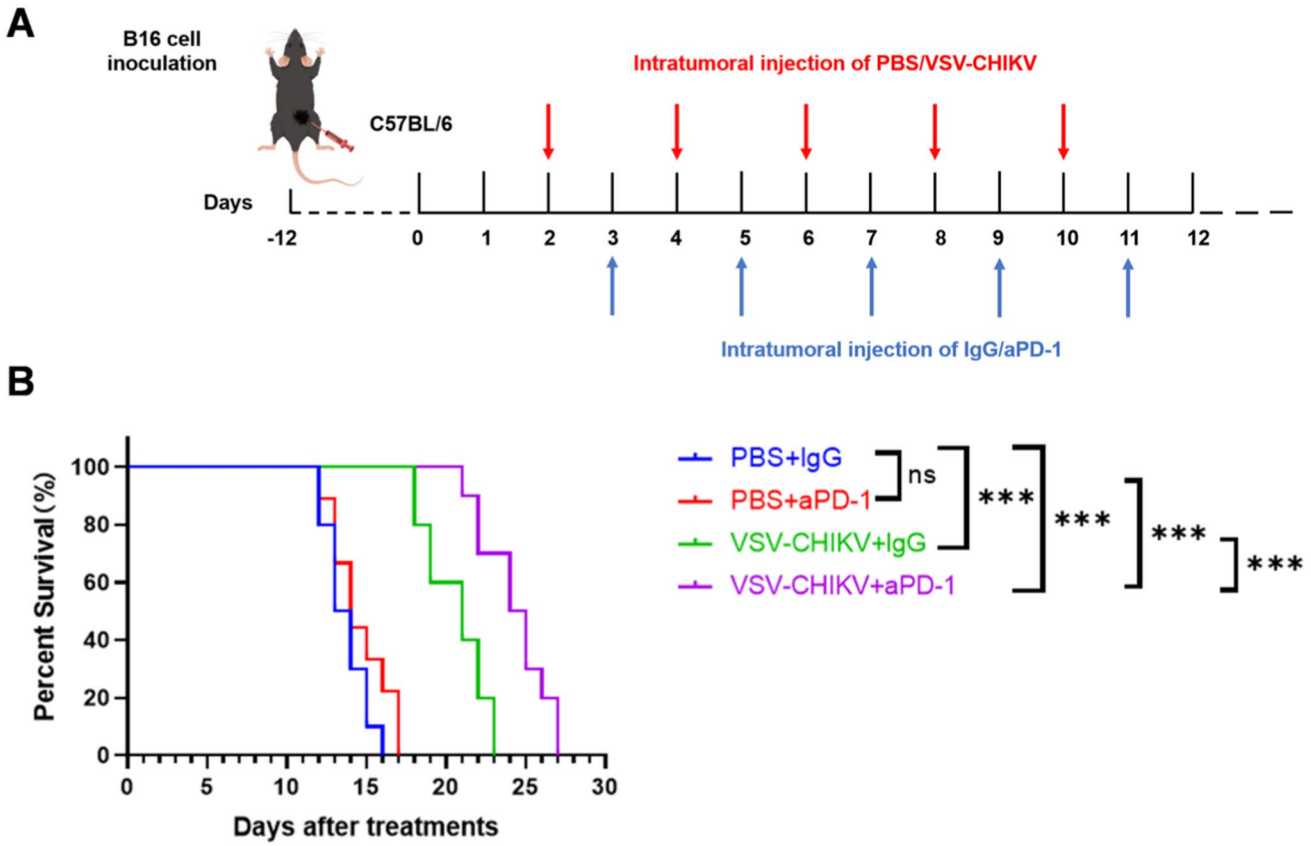

Fig. 6 VSV-CHIKV-based virotherapy enhances the efficacy of immune checkpoint blockade. **A** Schematic illustration of the experimental design. B16 cell tumor-bearing C57BL/6 mice were intratumorally treated with VSV-CHIKV and intraperitoneally treated with aPD-1 (5 mg/kg). **B** Kaplan–Meier survival curves were generated (n = 10)

anti-PD-1 antibody monotherapy did not affect the survival of immunologically "cold" homozygous mice. When the mice were pretreated with VSV-CHIKV, the anti-PD-1 antibody further significantly prolonged survival (Fig. 6B), which further suggested that the combination of VSV-CHIKV and anti-PD-1 antibody has better therapeutic efficacy in treating B16.

4 Discussion

VSV has been widely used as a vector for OV, and VSV has a broad host range and unique immunostimulatory ability, which is a natural advantage for the treatment of tumors [29]. However, the glycoprotein G protein of VSV is neurotoxic, so modification and optimization of wild-type VSV are needed. In this study, we found that recombinant VSV-CHIKV triggered GSDMD-mediated melanoma cell pyroptosis. Importantly, the NLRP3/Caspase-1/GSDMD axis was activated after VSV-CHIKV infection in melanoma cell lines and in a xenograft mouse model. Inhibition of GSDMD blocked cell pyroptosis, antitumor immunity and the tumor response in response to VSV-CHIKV treatment, suggesting that VSV-CHIKV acts through the GSDMD pathway (Fig. 7).

Traditionally, OVs are thought to kill tumors by inducing apoptosis [30]. Oncolytic VSV and its recombinants have been well characterized in current literature to efficiently induce apoptosis within 48 h post-infection, through the viral matrix (M) protein. GMCSF transgene armed VSVd51 (M mutant VSV) is found to induce enhanced immunogenic cell death [31]. However, apoptosis leads to immune quiescence, which is incompatible with the ability of OVs to activate the antitumor immune microenvironment. Cell apoptosis is essentially an immune tolerance process; in contrast, pyroptosis is characterized predominantly by the formation of gasdermin protein family-mediated membrane perforation and the consecutive release of pro-inflammatory cytokines. Canonical and non-canonical inflammasome activation of caspase-1/11 (mouse) or caspase-1/4/5 (human) leads to gasdermin D (GSDMD) cleavage and maturation of IL-1β and IL-18, and then the GSDMD-N domain causes pyroptosis by promoting the formation of membrane pores and the release

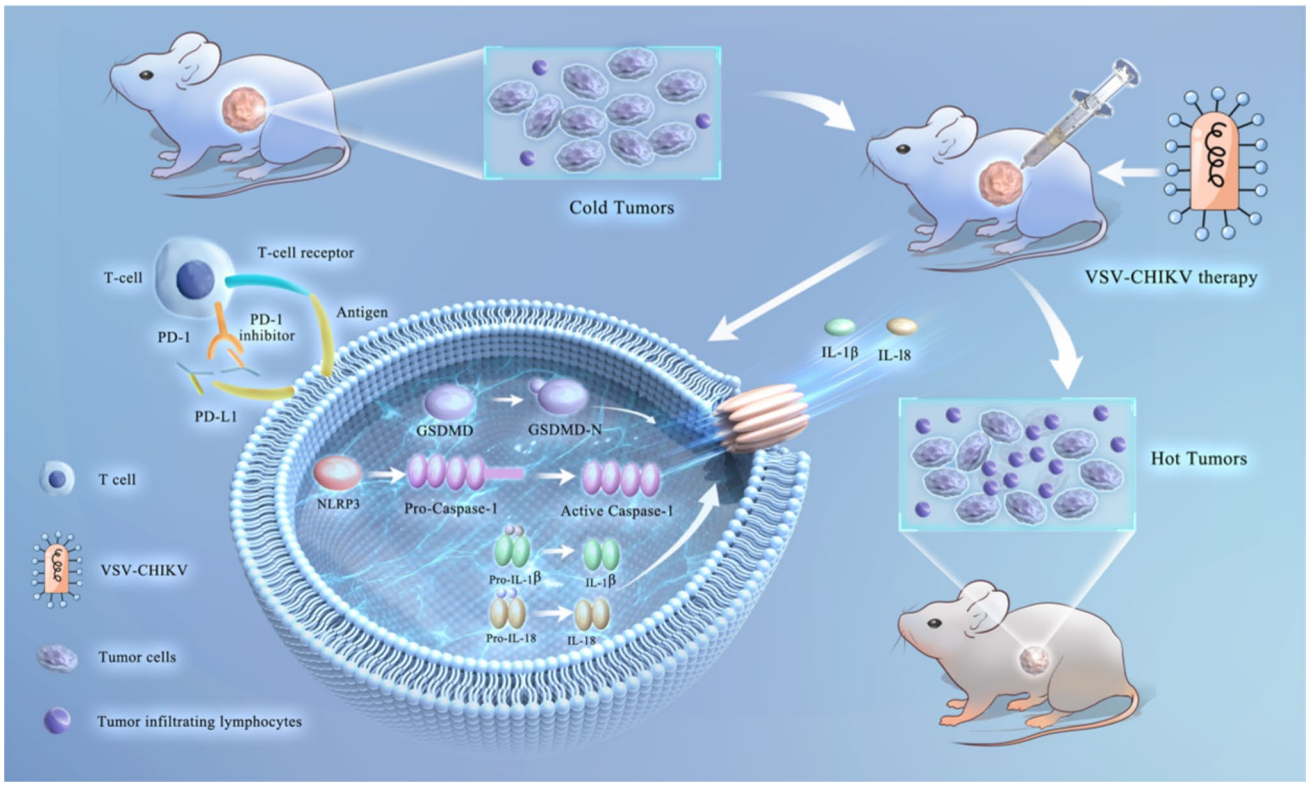

Fig. 7 VSV-CHIKV induces GSDMD-mediated pyroptosis and activates antitumor immunity. The NLRP3/Caspase-1/GSDMD axis was activated after melanoma cell lines were infected with VSV-CHIKV. VSV-CHIKV-triggered GSDMD-mediated tumor pyroptosis recruits CTLs into the tumor microenvironment, which is accompanied by the release of inflammatory mediators. This remodels the tumor microenvironment and turns immunologically "cold" tumors into "hot" tumors, thereby sensitizes these tumors to checkpoint blockade

of pro-inflammatory cytokines [32]. The pyroptosis of a small number of tumor cells is sufficient to trigger inflammatory reactions, thereby promoting immune activation of the tumor microenvironment and activating the antitumor immune response of T cells [33]. This study first verified the activation of the classical GSDMD-mediated pyroptosis pathway after the addition of VSV-CHIKV to melanoma cells, and further confirmed that GSDMD is a determinant of VSV-CHIKV-induced pyroptosis by adding the GSDMD inhibitor LDC7559. In summary, we emphasize that the oncolytic virus VSV-CHIKV induces pyroptosis in melanoma cells via the NLRP3/Caspase-1/GSDMD pathway.

The tumor microenvironment (TME) contains numerous intrinsic and adaptive immune cells that interact and regulate each other to form a unique immune microenvironment that influences tumorigenesis, progression, and the response to immunotherapy [34, 35]. Cytotoxic $CD8^+$ T cells (CTLs) in the TME are essential for the suppression and clearance of tumor cells; however, due to the influence of the tumor microenvironment, $CD8^+$ T cells are often incompetent and depleted and cannot be effectively activated, affecting the antitumor immune response [36]. In contrast, in this study, an increase in $CD8^+$ T cells was detected by flow cytometry after VSV-CHIKV infection compared to that in the mock group. The pyroptosis effector molecule GSDMD was identified as a facilitating factor affecting the antitumor effect of CD8+T cells in the tumor microenvironment, thus revealing the important role of pyroptosis in the modulation of CD8+T cells and antitumor immune responses. The efficacy of a single treatment is limited, and eliminating tumors completely by relying on oncolytic virus alone is difficult; moreover, oncolytic viruses often need to be used in combination with other therapies [37]. When immunotherapy was first discovered, it was called an immune checkpoint, namely PD-1 and PD-L1. PD-1 is expressed by T cells and is related to tumor cells, and tumor cells themselves can express PD-L1. When PD-1 is combined with PD-L1, it can inhibit the function of T cells in the body, preventing the discovery of tumor cells and resulting in continuous proliferation of tumor cells [38]. This study used a combination therapy of VSV-CHIKV and immune checkpoint inhibitor (anti PD-1) to treat cancer, and found that it prolonged the survival of mice.

Notably, VSV-CHIKV-based studies still have limitations. First, the viral proteins affecting the tumor lysis ability of VSV-CHIKV have been less well studied, and the key components remain to be explored. Second, specific antitumor immune responses and changes in macrophage polarization in the tumor microenvironment have not been detected. Based

on the above limitations, we will carry out exploratory work in the future, hoping that further in-depth studies of this oncolytic virus can solve additional problems in future clinical applications. In summary, the VSV-CHIKV strategy can be an attractive biologic therapy against melanoma, either as monotherapy or in combination with immune checkpoint inhibitors.

Acknowledgements None.

Author contributions All authors contributed to the study conception and design. Shibin Yu and Yingfeng Lei designed the study, and reviewed and modified the article. Fan Wu, Ying Zhan and Siyu Wang performed the main experiments as well as organized data and wrote the article. Xiaoke Wang, Min Hui, Jian Zhang, Jing Zhang and Hongxu Yang assisted in some experiments. All authors commented on previous versions of the manuscript. All authors read and approved the final manuscript.

Funding This work was supported by the National Natural Science Foundation of China (No. 82271000), Shaanxi Province Science Foundation (No. 2022JZ-52). The funders had no role in study design, data collection and analysis, the decision to publish this manuscript or the preparation of this manuscript.

Data availability Data is provided within the manuscript or supplementary information files.

Declarations

Ethical approval Animal experiments were approved by the Animal care & Welfare Committee, School of Stomatology, Fourth Military Medical University (kq-2022–020) and followed the ARRIVE guidelines. All methods were performed in accordance with relevant guidelines and regulations.

Consent to participate Not applicable.

Consent for publication Not applicable.

Competing interests The authors declare no competing interests.

References

1. Long GV, Swetter SM, Menzies AM, Gershenwald JE, Scolyer RA. Cutaneous melanoma. Lancet. 2023
2. Centeno PP, Pavet V, Marais R. The journey from melanocytes to melanoma. Nat Rev Cancer. 2023;23(6):372–90.
3. Kalaora S, Nagler A, Wargo JA, Samuels Y. Mechanisms of immune activation and regulation: lessons from melanoma. Nat Rev Cancer. 2022;22(4):195–207.
4. Kaufman HL, Kohlhapp FJ, Zloza A. Oncolytic viruses: a new class of immunotherapy drugs. Nat Rev Drug Discov. 2015;14(9):642–62.
5. Fukuhara H, Ino Y, Todo T. Oncolytic virus therapy: a new era of cancer treatment at dawn. Cancer Sci. 2016;107(10):1373–9.
6. Bommareddy PK, Aspromonte S, Zloza A, Rabkin SD, Kaufman HL. MEK inhibition enhances oncolytic virus immunotherapy through increased tumor cell killing and T-cell activation. Sci Transl Med. 2018;10(471): eaau0417.
7. Bommareddy PK, Patel A, Hossain S, Kaufman HL. Talimogene Laherparepvec (T-VEC) and other oncolytic viruses for the treatment of melanoma. Am J Clin Dermatol. 2017;18(1):1–15.
8. Shalhout SZ, Miller DM, Emerick KS, Kaufman HL. Therapy with oncolytic viruses: progress and challenges. Nat Rev Clin Oncol. 2023;20(3):160–77.
9. Andtbacka RHI, Kaufman HL, Collichio F, Amatruda T, Senzer N, Chesney J, Delman KA, Spitler LE, Puzanov I, Agarwala SS, Milhem M, Cranmer L, Curti B, Lewis K, Ross M, Guthrie T, Linette GP, Daniels GA, Harrington K, Middleton MR, Miller WH, Zager JS, Ye Y, Yao B, Li Ai, Doleman S, VanderWalde A, Gansert J, Coffin RS. Talimogene Laherparepvec improves durable response rate in patients with advanced melanoma. J Clin Oncol. 2015;33(25):2780–8.
10. Orzechowska BU, Jędryka M, Zwolińska K, Matkowski R. VSV based virotherapy in ovarian cancer: the past, the present and …future? J Cancer. 2017;8(12):2369–83.
11. Chattopadhyay A, Wang E, Seymour R, Weaver SC, Rose JK. A chimeric vesiculo/alphavirus is an effective alphavirus vaccine. J Virol. 2013;87(1):395–402.

12. Voss JE, Vaney M-C, Duquerroy S, Vonrhein C, Girard-Blanc C, Crublet E, Thompson A, Bricogne G, Rey FA. Glycoprotein organization of Chikungunya virus particles revealed by X-ray crystallography. Nature. 2010;468(7324):709–12.
13. Yap ML, Klose T, Urakami A, Hasan SS, Akahata W, Rossmann MG. Structural studies of Chikungunya virus maturation. Proc Natl Acad Sci USA. 2017;114(52):13703–7.
14. Uchime O, Fields W, Kielian M. The role of E3 in pH protection during alphavirus assembly and exit. J Virol. 2013;87(18):10255–62.
15. Taylor A, Melton JV, Herrero LJ, Thaa B, Karo-Astover L, Gage PW, Nelson MA, Sheng K-C, Lidbury BA, Ewart GD, McInerney GM, Merits A, Mahalingam S. Effects of an in-frame deletion of the 6k gene locus from the genome of ross river virus. J Virol. 2016;90(8):4150–9.
16. Zhang X, Mao G, van den Pol AN. Chikungunya-vesicular stomatitis chimeric virus targets and eliminates brain tumors. Virology. 2018;522:244–59.
17. Kao Y-T, Wang H-I, Shie C-T, Lin C-F, Lai MMC, Chia-Yi Yu. Zika virus cleaves GSDMD to disseminate prognosticable and controllable oncolysis in a human glioblastoma cell model. Mol Ther Oncolytics. 2023;28:104–17.
18. Ding J, Wang K, Liu W, She Y, Sun Qi, Shi J, Sun H, Wang D-C, Shao F. Pore-forming activity and structural autoinhibition of the gasdermin family. Nature. 2016;535(7610):111–6.
19. Broz P, Pelegrín P, Shao F. The gasdermins, a protein family executing cell death and inflammation. Nat Rev Immunol. 2020;20(3):143–57.
20. Wang K, Sun Qi, Zhong X, Zeng M, Zeng H, Shi X, Li Z, Wang Y, Zhao Q, Shao F, Ding J. Structural mechanism for GSDMD targeting by autoprocessed caspases in pyroptosis. Cell. 2020;180(5):941-955.e20.
21. Wang G, Li J, Bojmar L, Chen H, Li Z, Tobias GC, Hu M, Homan EA, Lucotti S, Zhao F, Posada V, Oxley PR, Cioffi M, Kim HS, Wang H, Lauritzen P, Boudreau N, Shi Z, Burd CE, Zippin JH, Lo JC, Pitt GS, Hernandez J, Zambirinis CP, Hollingsworth MA, Grandgenett PM, Jain M, Batra SK, DiMaio DJ, Grem JL, Klute KA, Trippett TM, Egeblad M, Paul D, Bromberg J, Kelsen D, Rajasekhar VK, Healey JH, Matei IR, Jarnagin WR, Schwartz RE, Zhang H, Lyden D. Tumour extracellular vesicles and particles induce liver metabolic dysfunction. Nature. 2023;618(7964):374–82.
22. Chen X, Lu Q, Zhou H, Liu J, Nadorp B, Lasry A, Sun Z, Lai B, Rona G, Zhang J, Cammer M, Wang K, Al-Santli W, Ciantra Z, Guo Q, You J, Sengupta D, Boukhris A, Zhang H, Liu C, Cresswell P, Dahia PLM, Pagano M, Aifantis I, Wang J. A membrane-associated MHC-I inhibitory axis for cancer immune evasion. Cell. 2023;186(18):3903–20.
23. He F, Ma Y, Li S, Ren H, Liu Q, Chen X, Miao H, Ye T, Lu Q, Yang Z, Li T, Tong X, Yang H, Zhang M, Wang H, Wang Y, Yu S. Necroptotic TNFα-Syndecan 4-TNFα vicious cycle as a therapeutic target for preventing temporomandibular joint osteoarthritis. J Bone Miner Res. 2022;37(5):1044–55.
24. Wang Q, Gao H, Clark KM, Mugisha CS, Davis K, Tang JP, Harlan GH, DeSelm CJ, Presti RM, Kutluay SB, Shan L. CARD8 is an inflammasome sensor for HIV-1 protease activity. Science. 2021. https://doi.org/10.1126/science.abe1707.
25. Bedient L, Pokharel SM, Chiok KR, Mohanty I, Beach SS, Miura TA, Bose S. Lytic cell death mechanisms in human respiratory syncytial virus-infected macrophages: roles of pyroptosis and necroptosis. Viruses. 2020;12(9):392.
26. Kuriakose T, Man SM, Subbarao Malireddi RK, Karki R, Kesavardhana S, Place DE, Neale G, Vogel P, Kanneganti T-D. ZBP1/DAI is an innate sensor of influenza virus triggering the NLRP3 inflammasome and programmed cell death pathways. Science Immunol. 2016. https://doi.org/10.1126/sciimmunol.aag2045.
27. Walle LV, Lamkanfi M. Snapshot of a deadly embrace: the caspase-1-GSDMD interface. Immunity. 2020;53(1):6–8.
28. Curran MA, Montalvo W, Yagita H, Allison JP. PD-1 and CTLA-4 combination blockade expands infiltrating T cells and reduces regulatory T and myeloid cells within B16 melanoma tumors. Proc Natl Acad Sci USA. 2010;107(9):4275–80.
29. Bishnoi S, Tiwari R, Gupta S, Byrareddy SN, Nayak D. Oncotargeting by vesicular stomatitis virus (VSV): advances in cancer therapy. Viruses. 2018;10(2):90.
30. Twumasi-Boateng K, Pettigrew JL, Eunice Kwok Y, Bell JC, Nelson BH. Oncolytic viruses as engineering platforms for combination immunotherapy. Nat Rev Cancer. 2018;18(7):419–32.
31. Larrieux A, Sanjuán R. Cellular resistance to an oncolytic virus is driven by chronic activation of innate immunity. iScience. 2023;26(1):105749.
32. Ma R, Zhenlong Li E, Chiocca A, Caligiuri MA, Jianhua Yu. The emerging field of oncolytic virus-based cancer immunotherapy. Trends Cancer. 2023;9(2):122–39.
33. Wang Q, Wang Y, Ding J, Wang C, Zhou X, Gao W, Huang H, Shao F, Liu Z. A bioorthogonal system reveals antitumor immune function of pyroptosis. Nature. 2020;579(7799):421–6.
34. Feng M, Jiang W, Kim BYS, Zhang CC, Yang-Xin Fu, Weissman IL. Phagocytosis checkpoints as new targets for cancer immunotherapy. Nat Rev Cancer. 2019;19(10):568–86.
35. Zhang Y, Zhang Z. The history and advances in cancer immunotherapy: understanding the characteristics of tumor-infiltrating immune cells and their therapeutic implications. Cell Mol Immunol. 2020;17(8):807–21.
36. John Wherry E, Kurachi M. Molecular and cellular insights into T-cell exhaustion. Nat Rev Immunol. 2015;15(8):486–99.
37. Rezaei R, Ghaleh HEG, Farzanehpour M, Dorostkar R, Ranjbar R, Bolandian M, Nodooshan MM, Alvanegh AG. Combination therapy with CAR T cells and oncolytic viruses: a new era in cancer immunotherapy. Cancer Gene Ther. 2022;29(6):647–60.
38. Engeland CE, Grossardt C, Veinalde R, Bossow S, Lutz D, Kaufmann J, Shevchenko I, Umansky V, Nettelbeck DM, Weichert W, Jäger D, von Kalle C, Ungerechts G. CTLA-4 and PD-L1 checkpoint blockade enhances oncolytic measles virus therapy. Mol Ther. 2014;22(11):1949–59.